

Finite element analysis of mechanical impacts in large imaging detectors

Li Ma¹, Weibo Li², Hengwen Zhang^{2,*}, and Chunqiu Wang³

¹China Electronics Standardization Institute, Beijing 100007, China

²School of Intelligent Engineering and Automation, Beijing University of Posts and Telecommunications, Beijing 102206, China

³International School, Beijing University of Posts and Telecommunications, Beijing 100876, China

Abstract. This study utilizes Ansys to analyze the stress distribution of a large imaging detector subjected to mechanical impacts, including vibration, shock loading, and collision, encountered during space missions. Employing an axisymmetric model and direct solution method, the study simulates the detector's stress-deformation field. Results indicate that during impact, maximum stresses on both the chip and its adhesive concentrate at the edge region, remaining within safe limits. Furthermore, simulations demonstrate a positive correlation between detector size and stress magnitude. Notably, the adhesive effectively reduces stress concentration at the chip's center. These analyses offer valuable insights for optimizing the detector's structural design and mitigating potential weaknesses during the manufacturing process.

1 Introduction

Photodetectors are semiconductor devices that leverage the photoelectric effect to convert optical signals into electrical signals. They are categorized based on their spectral sensitivity, encompassing visible, infrared, and ultraviolet detectors. Applications span diverse fields, including military, aerospace, and energy sectors.

The primary mechanical shock challenges for space probes include:

Vibration: Spacecraft experience various vibrational modes during launch and flight operations. These vibrations can induce detrimental effects on detector performance, including reduced accuracy, compromised stability, and inaccurate data acquisition.

Shock Loads: Spaceborne photodetectors are vulnerable to damage from transient shock loads during launch, re-entry, or turbulence, which can harm internal components or cause complete failure.

Collision and contact: Physical collisions or unintended contact during ground handling, integration, or in-orbit operations can also inflict damage on photodetectors. Mishandling or unforeseen events may result in structural degradation or functional impairment.

* Corresponding email: zhanghengwen@bupt.edu.cn

2 Modelling and mechanical models

2.1 External dimensions of devices

The device is hermetically sealed in a PGA522 ceramic shell package. The device form factor and dimensions are illustrated in Figure 1. and Table 1.

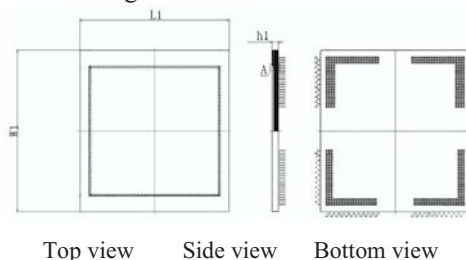


Fig. 1. Device package structure.

Table 1. Device external dimensions.

Size Symbol	L1	W1	In millimetres h1
minimum value	153.50	167.00	6.00
nominal value	155.00	168.00	6.50
maximum values	156.50	169.00	7.00

The detector comprises five main components: chip, glass cover, cover plate adhesive, base, and chip adhesive. To facilitate stress analysis and simplify the model, subsequent sections focus solely on these five components.

2.2 Chip and image plane dimensions

The dimensions of the chip and the image plane are illustrated in Figure 2.:

Chip dimensions: $(131.91 \pm 0.10) \text{ mm} \times (131.00 \pm 0.10) \text{ mm}$

Image plane dimensions: $(121.80 \pm 0.10) \text{ mm} \times (121.80 \pm 0.10) \text{ mm}$.

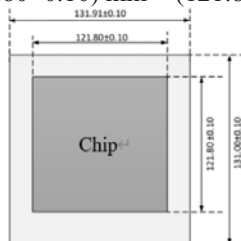


Fig. 2. Schematic diagram of device structure and image plane dimensions.

2.3 Mechanical model

Upon experiencing mechanical impact, the chip is subjected to an instantaneous impulse load, resulting in vibrations and inducing compressive stress and deformation. The presence of the chip adhesive partially absorbs the impact energy, significantly attenuating the load transmitted to the chip while simultaneously generating a minor tensile stress on the chip. Due to the chip's embedment within the substrate and the difference in their Poisson's ratios, the surrounding regions of the chip also experience stress waves originating from the

substrate during impact. Consequently, the maximum stress concentration occurs at the periphery of the chip and the chip adhesive, as depicted in Figure 3.



Fig. 3. Schematic diagram of the chip stresses.

Formula for calculation of principal stresses^[3]:

$$\sigma_1 = \frac{I_1}{3} + 2\sqrt{-\frac{p}{3} \cos \frac{\theta}{3}} \tag{1}$$

$$\sigma_2 = \frac{I_1}{3} - \sqrt{-\frac{p}{3} \left(\cos \frac{\theta}{3} - \sqrt{3} \sin \frac{\theta}{3} \right)} \tag{2}$$

$$\sigma_3 = \frac{I_1}{3} - \sqrt{-\frac{p}{3} \left(\cos \frac{\theta}{3} + \sqrt{3} \sin \frac{\theta}{3} \right)} \tag{3}$$

where : $\theta = \arccos \left[-\frac{q}{2} \left(-\frac{p^3}{27} \right)^{\frac{1}{2}} \right] (0 < \theta < \Pi)$

$$p = \frac{3I_2 - I_1^2}{3}$$

$$q = \frac{9I_1I_2 - 2I_1^3 - 27I_3}{27}$$

$$I_1 = \sigma_x + \sigma_y + \sigma_z$$

$$I_2 = \sigma_x\sigma_y + \sigma_y\sigma_z + \sigma_z\sigma_x - \tau_{xy}^2 - \tau_{yz}^2 - \tau_{zx}^2$$

$$I_3 = \sigma_x\sigma_y\sigma_z + 2\tau_{xy}\tau_{yz}\tau_{zx} - \sigma_x\tau_{yz}^2 - \sigma_y\tau_{zx}^2 - \sigma_z\tau_{xy}^2$$

Under certain conditions of deformation, when the second invariant J_2' of the stress bias tension at a point within the stressed object reaches a certain value, the point enters into the plastic state.

$$(\sigma_x - \sigma_y)^2 + (\sigma_y - \sigma_z)^2 + (\sigma_z - \sigma_x)^2 + 6(\tau_{xy}^2 + \tau_{yz}^2 + \tau_{zx}^2) = 2\sigma_s^2 = 6K^2 \tag{4}$$

σ_s is the yield point of the material

K is the shear yield strength of the material

σ_x is the positive stress on the X-axis

σ_y is the positive stress on the Y-axis

σ_z is the positive stress in the Z-axis

τ_{xy} is the tangential stress in the X-axis towards the Y-axis

τ_{yz} is the tangential stress in the Y-axis towards the Z-axis

τ_{zx} is the shear stress in the Z-axis towards the X-axis

Comparison with the equivalent force gives

$$\bar{\sigma} = \frac{1}{\sqrt{2}} \sqrt{(\sigma_x - \sigma_y)^2 + (\sigma_y - \sigma_z)^2 + (\sigma_z - \sigma_x)^2 + 6(\tau_{xy}^2 + \tau_{yz}^2 + \tau_{zx}^2)} = \sigma_s \tag{5}$$

The strength condition for the failure criterion is:

$$\frac{1}{\sqrt{2}} \sqrt{(\sigma_1 - \sigma_2)^2 + (\sigma_2 - \sigma_3)^2 + (\sigma_3 - \sigma_1)^2} \leq [\sigma] \tag{6}$$

3 Finite element simulation

3.1. Analytical model

A mass encapsulated imaging photodetector comprises five key structural elements: an optical window (hereinafter referred to as the cover plate), a tube shell (substrate), a cover plate adhesive, a chip, and a chip adhesive.

Given the detector's axisymmetric geometry, a bottom-up modeling methodology was adopted. The substrate was initially generated by extruding a series of points into lines and subsequently into surfaces. The remaining components were then formed by strategically extruding and trimming the substrate.

To enhance computational accuracy and expedite convergence, a multi-region meshing strategy was implemented for the large-scale imaging photodetector package. Hexahedral elements were utilized throughout the model, with localized mesh refinement applied to the two thin adhesive layers. The element size within the adhesive layers was constrained to 0.02 mm, while a coarser mesh with an element size of 0.5 mm was employed in the remaining regions to minimize computational burden.

3.2. Solution method

A direct solver was selected due to its compatibility with the mesh structure and its capacity to enhance solution efficiency. The solver employed a Newton-Raphson iterative scheme to impose a prescribed downward displacement and obtain the resultant stress-deformation field following mechanical impact.

Table 2. Material parameters.

	Density (kg/m ³)	Young's modulus (GPa)	Poisson's ratio
Sapphire glass	4000	524	0.28
Aluminum trioxide	3960	350	0.25
Gallium arsenide	5320	84.8	0.31
Epoxy resin (chemistry)	1160	1	0.38
Silver paste	10500	73.2	0.38

3.3 GJB Mechanical shock related provisions

The device body shall be subjected to a specified half-sine shock pulse characterized by a peak acceleration between 4900 m/s² and 294000 m/s² and a pulse duration ranging from 0.1 ms to 1.0 ms. The Y1 direction is defined as the direction in which the element tends to separate from its base. The element shall undergo five shock pulses in the Y1 direction under test condition B.

3.4 Material parameters

Cover: sapphire glass; Substrate: aluminum trioxide; Chip: gallium arsenide; Cover adhesive: epoxy resin; Chip adhesive: silver paste.

3.5 Boundary conditions for the detector

A shock pulse of 14700 (1500 g) m / s^2 (peak acceleration) with a pulse width of 0.5 ms

was applied to the detector in the Y1 direction, and the shock wave was a half-sine wave.

3.6 Simulation results

The distributions of peak stress in the chip and chip adhesive following five half-sine wave impacts are illustrated in Figure 4. Analysis of the chip stress distribution reveals that the maximum stress, reaching 2.116 MPa, is concentrated at the chip periphery.

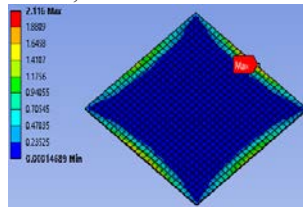


Fig. 4. Cloud diagram of chip stress distribution.

Analysis of the chip adhesive stress distribution reveals that the maximum stress, reaching 1.3789 MPa, is concentrated at the adhesive periphery.

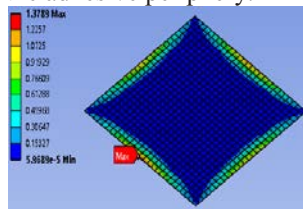


Fig. 5. Cloud view of chip glue stress distribution.

3.7 Zoom-in/Zoom-out simulation and results for this model of detector

(1) 0.5 times

The distributions of peak stress in the chip and chip adhesive following five half-sine wave impacts are illustrated in Figure 6. Analysis of the chip stress distribution reveals that the maximum stress, reaching 0.33633 MPa, is concentrated at the chip periphery.

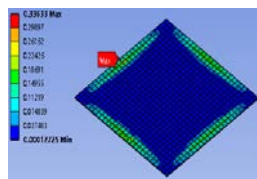


Fig. 6. Cloud view of 0.5x chip stress distribution.

Analysis of the chip adhesive stress distribution reveals that the maximum stress, reaching 0.20021 MPa, is concentrated at the adhesive periphery.

(2) 2 times

The distributions of peak stress in the chip and chip adhesive following five half-sine wave impacts are illustrated in Figure 8. Analysis of the chip stress distribution reveals that the maximum stress, reaching 2.5809 MPa, is concentrated at the chip periphery.

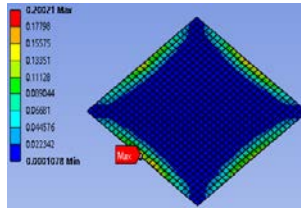


Fig. 7. Cloud view of 0.5x chip glue stress distribution.

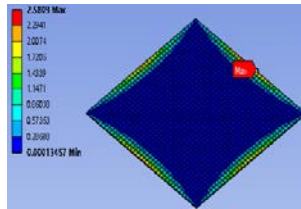


Fig. 8. Cloud view of 2x chip stress distribution.

Analysis of the chip adhesive stress distribution reveals that the maximum stress, reaching 1.9853 MPa, is concentrated at the adhesive periphery.

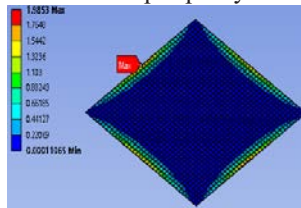


Fig. 9. Cloud view of 2x chip glue stress distribution.

3.8 Analysis of simulation results

1. Both the maximum stress and maximum deformation occur at the periphery of the chip and chip adhesive.
2. Under identical half-sine wave impact conditions, stress magnitude is directly proportional to detector size. Larger detectors experience greater stress.
3. Simulation results indicate that both the chip and chip adhesive remain within their respective stress limits, confirming a safe operating range.

4 Conclusion

Analysis of the large photodetector's structure and materials, which consist of various materials with distinct parameters, combined with stress results derived under mechanical impact conditions, yields the following conclusions:

1. During mechanical impact, stress fluctuates cyclically between maximum and minimum values. Within the normal permissible range, the difference between these peak and trough stress values is minimal, posing no threat of damage to the detector. Maximum stress occurs at peak acceleration, concentrated around the chip periphery and exhibiting cyclic variations aligned with the half-sine wave profile.
2. Stress distribution varies across different components due to variations in material parameters.

3. Detector size directly influences stress magnitude under half-sine wave impact. Larger detectors experience greater stress.

4. Upon impact load application, the chip adhesive significantly mitigates stress at the chip center, although the overall stress reduction at this location is not substantial. The chip's embedment within the substrate leads to stress wave transmission from the substrate, primarily impacting the chip periphery. This explains the concentration of maximum stress at the periphery of both the chip and chip adhesive. Therefore, analyzing the mechanical impact response of individual components within large photodetectors provides valuable insights for optimizing subsequent design and manufacturing processes, particularly for mitigating weaknesses in critical areas.

Reference

1. R. Yu, L. Cheng and D. Zhang, "On-Chip Generation Method of Shock Load and Characterization of Microstructure Shock Process," in *Journal of Microelectromechanical Systems*, vol. 31, no. 4, pp. 712-720, Aug. 2022, doi: 10.1109/JMEMS.2022.3180411.
2. J. Fan et al., "Fatigue Damage Assessment of LED Chip Scale Packages with Finite Element Simulation," 2018 19th International Conference on Electronic Packaging Technology (ICEPT), Shanghai, China, 2018, pp. 1642-1648, doi: 10.1109/ICEPT.2018.8480748.
3. K Wang. Calculation Formulas For Principal Stresses[J]. *Mechanic in Engineering* 2014, 36(6): 783-785. DOI: 10.6052/1000-0879-13-502.
4. Tzu-Hsuan Cheng, H. -C. Cheng, W. -H. Chen, Hsin-Yi Huang and Tao-Chih Chang, "Reliability characterization of 2.5D multi-chip module on board under drop impact," 2014 International Conference on Electronics Packaging (ICEP), Toyama, 2014, pp. 215-218, doi: 10.1109/ICEP.2014.6826691.
5. Z. Wang, C. Xie, C. Wang and X. Wang, "Investigation on the Vibration Amplitude of Au Bonding Wire Under Mechanical Shock," 2018 IEEE International Symposium on the Physical and Failure Analysis of Integrated Circuits (IPFA), Singapore, 2018, pp. 1-4, doi: 10.1109/IPFA.2018.8452563.
6. C. -S. Lau, N. Ye and H. Takiar, "A Response Spectrum Method and Post-layout Optimization for Mechanical Shock Analysis of 3D NAND BGA Packages," 2018 IEEE CPMT Symposium Japan (ICSJ), Kyoto, Japan, 2018, pp. 1-4, doi: 10.1109/ICSJ.2018.8602610.
7. J. Gu, W. Xie, C. Guirguis, M. Ahmad and Y. Pang, "System level mechanical shock reliability of BGA packages: Experimental and numerical analysis," 2017 18th International Conference on Electronic Packaging Technology (ICEPT), Harbin, China, 2017, pp. 1163-1168, doi: 10.1109/ICEPT.2017.8046647.
8. J. Gu, W. Xie, M. Ahmad and Q. Wang, "Experimentally validated analysis and parametric optimization of mechanical shock testing of advanced BGA packages," 2015 16th International Conference on Electronic Packaging Technology (ICEPT), Changsha, China, 2015, pp. 501-507, doi: 10.1109/ICEPT.2015.7236636.